Hydrogen diffusion and trapping in a steel containing porosities

Ahmed Yaktiti, Alixe Dreano, J.F. Carton, Frédéric Christien

Hydrogen diffusion and trapping in a steel containing porosities

A. Yaktiti[1,2], A. Dreano[1], J.F Carton[2], F. Christien[1]

[1] Mines Saint-Etienne, Univ Lyon, CNRS, UMR 5307 LGF, Centre SMS, F-42023, Saint-Etienne, France

[2] SafeMetal, 1 Boulevard de la Boissonnette, 42110 Feurs, France

Abstract

The effect of porosity on diffusion and trapping of hydrogen in a cast steel was studied using electrochemical permeation (EP) and thermal desorption spectrometry (TDS). A comparison between porous and non-porous samples of the same material was conducted. It was demonstrated that hydrogen was mainly located in cavities. Those cavities behave as reversible traps at room temperature. In addition, hydrogen content increases linearly with increasing volume fraction of porosity. Finally, a method was proposed to estimate the hydrogen fugacity of the solution used for chemical charging, as well as the hydrogen solubility of the material.

Keywords

I Introduction

It has been well proved that hydrogen represents a harmful element for steels because it leads to a serious decrease in mechanical properties, especially loss of ductility [1][2][3]. This phenomenon is known as Hydrogen Embrittlement (HE) [4].

Different HE mechanisms are described in literature [5], among them the hydrogen pressure theory firstly introduced by Zapffe in 1941 [6]. In this work, a special focus was set on this mechanism because cast steels usually have porosity defects. The formation of these defects is due to the volume shrinkage and the gas evolution during the solidification process [7][8]. Therefore, it is very important to understand the effect of porosity on HE phenomena.

The hydrogen pressure theory is a HE mechanism in which atomic hydrogen H diffuses through the material and recombines as molecular hydrogen H_2 inside the cavities. As a result, the internal pressure rises and it keeps rising as atomic hydrogen continues to diffuse until reaching equilibrium between the lattice hydrogen and the hydrogen within the cavity. The pressure can attain hundreds of MPa in some cases [9] and it generates a stress field around the cavity, which can lead to rupture [6][10][11]. The internal pressure cannot be measured experimentally.

The hydrogen induced in cast steels is mainly the result of chemical reactions that took place during the manufacturing process, between the molten steel and the water vapor. The hydrogen uptake can be very important because of the high solubility of hydrogen in the molten steel [12]. The solubility rises greatly from the solid state to the liquid state and it increases with increasing temperature. In steel foundry, water vapor comes from different sources such as air humidity, additive materials, wet refractories, molds and charge materials [13].

In order to improve mechanical properties and to prevent brutal failures caused by HE [14], in other words to increase HE resistance, it is crucial to investigate hydrogen behavior in cast steels because hydrogen mobility and hydrogen trapping are very important to clearly understand HE mechanisms [15]. It is also important to note that many studies were performed to give a better understanding of hydrogen diffusion and trapping in steels

[16][17][18]. However, little work has been done for cast steels, and the studies that focused on the effect of porosities on hydrogen diffusion and trapping are rare. These few studies [19][20][21][22][23][24] mentioned that voids act as trapping sites for hydrogen. For instance, Choo and Lee worked with pure iron samples that have different densities and they determined a trapping energy of 35.2 kJ/mol for the microvoids through thermal desorption spectrometry (TDS) measurements [24]. However, the reversible or irreversible nature of these traps at room temperature is not entirely clear. Some studies mentioned that voids are reversible traps for hydrogen [19][20] while others considered them as irreversible traps [21][22][23]. Lee et al. worked on hydrogen trapping in nickel and pure iron. They concluded that voids act as strong trapping sites for hydrogen in both materials [21][22]. The nature of trapping by voids, in the case of cast steels, is discussed in details in this article.

Electrochemical permeation (EP) and TDS experiments are widely performed to study hydrogen mobility and trapping inside different materials [25][26]. In this study, these two techniques were used to closely investigate the influence of porosity on the hydrogen diffusion and trapping processes in a low-alloy cast steel. This work is based on a comparative study between porous samples (raw material) and non-porous samples (the same material but after forging). Finally, from the TDS data a method is proposed in order to calculate hydrogen fugacity of the charging solution used, as well as the hydrogen solubility (Sieverts constant) of the studied material.

II Material and experimental procedure

II.1 Material

The raw material provided for this study was an ingot of low-alloy cast steel (G20MN5). The alloy had been elaborated in an electric arc furnace and then the molten steel was poured in a sand mold. After slowly cooling at room temperature, the ingot was removed from the mold. The ingot dimensions were approximately 300x120x100 mm. The chemical composition of this steel is provided in Table 1. Finally, it is worth noting that no heat treatments were performed on this material until this point.

Table 1 : Chemical composition of the material used in this study

Element	C	Mn	Si	S	P	Ni	Cr	Mo	V
% mass	0.187	1.120	0.410	0.009	0.008	0.230	0.150	0.020	0.001

II.2   Forging and heat treatments

The ingot was sectioned along the length axis into two halves and then, each half was cut into parts of 250x52x45 mm. The bars from the first half were forged at 1000°C to a forging ratio of 3.4. The aim of the forging step was to close cavities in order to get a non-porous material. The final dimensions were 300x26x26 mm. The other bars were machined to obtain the same dimensions as the forged bars. In this way, the heat transfer behavior during subsequent heat treatments and quenching will be the same for the raw bars and the forged bars. Finally, in an attempt to have the same microstructure, all bars were normalized at 880°C for 60 minutes and then air cooled to room temperature. In the following sections, for convenience, the term ''forged'' is used for the "forged and normalized" material, and the term "cast" is used for the "cast and normalized" material.

II.3   X-ray tomography

X-ray tomography is a non-destructive technique used to reveal some internal features of materials. It is based on the absorption of X-rays through a specimen. It is widely used in several fields especially in medical and material sciences [27]. The principle is to acquire multiple radiographs while the specimen is rotating around an axis perpendicular to the X-ray beam. A reconstruction algorithm is then used to obtain a virtual volume of the scanned object, which allows to determine certain useful characteristics (porosity, defects size, distribution…). In this study, a Nanotom Phoenix X-ray tomography was used in order to characterize cavities in the cast samples and check the absence of cavities in the forged samples. The samples were small cylinders of 2 mm in diameter and 6 mm of height. With this diameter, the size resolution (i.e. the size of the smallest cavity that can be detected) is 1.5 µm. The scans were performed by applying a 160 kV voltage, 30 µA current and a 0.5 mm copper filter resulting in a pixel size of 1.5 µm. 1600 projections were recorded for each scan and the collected data were then analyzed and visualized using Avizo software.

II.4   Hydrostatic weighing technique

Hydrostatic weighing is a technique that has been widely used for the determination of the density of different solid materials [28]. This technique is based on Archimedes' principle. It consists in weighing a sample in air and then in a liquid with a well-known density. The weight in air represents the true weight and the weight in the liquid permits to determine the true volume of the sample. These two measurements permit to obtain the density of the sample and by comparing this latter to the true density of the material, it was possible to calculate the volume fraction of porosity.

In this study, the liquid used was pure ethanol (99.5%) and the resolution of the digital balance was 0.1 mg. Each measurement was performed three times. The temperature of the ethanol was determined each time in order to obtain its true density.

Considering the average mass of the specimens used in this study (4 g), the measurement uncertainty on the porosity fraction was estimated at ± 0.02%.

II.5   Electrochemical permeation

In this study, electrochemical permeation tests were performed in order to study hydrogen diffusion and trapping in cast and forged samples, using the method presented by Devanathan and Stachurski [29] [30].

The experimental setup is composed of two compartments. Each compartment was equipped with a saturated calomel reference electrode (SCE), a platinum auxiliary electrode and a common working electrode. The working electrode was a rectangular-shape specimen of the studied material. It was placed between the two cells and the specimen-electrolyte contact area was of 0.785 cm^2. Each compartment was filled with a 0.1 M NaOH aqueous solution that was deaerated by nitrogen bubbling before and during the whole test.

All permeation specimens were obtained from the normalized bars. They were ground on the two sides using emery paper up to 2500 grits followed by polishing with a 3 μm and 1 μm diamond paste. A good finish is actually needed here in order to keep surface roughness at minimum and actually obtain the targeted current density on the entry side. Just before mounting the specimen in the setup, they were cleaned in acetone and then ethanol. The final thickness of the specimen ranges from 1.96 mm to 1.80 mm.

All permeation tests were performed at room temperature and PGP201 Potentiostats were used. The entry side was galvanostatically polarized at -800 µA/cm² to introduce hydrogen. An anodic potential of -300mV/SCE, corresponding to +50 mV/OCP (open circuit potential) was applied on the exit side to oxidize hydrogen atoms reaching the exit surface.

The effective diffusion coefficient, D_{eff} (m^2/s) was calculated using the time lag method from the permeation rise transient [31]:

$$D_{eff} = \frac{e^2}{6t_l} \qquad (1)$$

where e is the sample thickness (m) and t_l (s) represents the time when the current density at the exit side is equal to 0.63 of the steady-state current density.

II.6   Chemical charging technique

A chemical charging method was used in this study to introduce hydrogen into materials samples. It consists in immersing samples in an ammonium thiocyanate (NH_4SCN) aqueous solution heated at 50°C. This method is largely used to evaluate HE susceptibility of prestressed concrete steels [32]. The amount of absorbed hydrogen can be modified by varying the NH_4SCN concentration of the solution.

In this study, rectangular plate samples (11x26x1.9 mm) were used for chemical hydrogen charging and subsequent TDS measurements. These samples were first cut from the forged and the cast bars and then they were polished with SiC paper up to 1200 grit. In contrast to electrochemical permeation where surface roughness must be kept at minimum to control the actual current density on the entry side, a 1200 grit finish was considered sufficient here, following the procedure detailed in [32]. Finally, they were cleaned with acetone just before the immersion in the NH_4SCN aqueous solution. After charging, the samples were polished once again with 1200 SiC paper and cleaned with acetone. In fact, during the immersion, a corrosion film forms. Consequently, it is very important to remove this layer before starting the TDS measurement in order to have trustworthy results because this layer can be a source of contamination. Finally, since the oxide layer was manually removed using SiC paper, the final thickness of the samples was not always the same. It ranged between 1.85 mm and 1.70 mm, which does not affect significantly the results.

II.7   Thermal desorption spectroscopy

TDS is commonly used to study gas desorption from metals [33][34]. It permits to determine the hydrogen trapping energies for different traps (grain boundaries, voids, dislocations…) as well as the hydrogen concentration in the analyzed samples [35][36]. In this study, the experiment consists in measuring the amount of desorbed hydrogen from a charged steel sample while a continuous heating is applied by means of a tubular furnace. The quantity of the desorbed hydrogen is obtained using a calibrated mass spectrometer. The TDS measurement output is a spectrum which represents an intensity (number of ions) as a function of time (or temperature). It should be mentioned that for hydrogen spectra, mass 2 (H_2) was monitored.

In this study, all the TDS measurements were performed using a Pfeiffer QMG 220 PrismaPlus mass spectrometer. All TDS samples were charged chemically (as explained in the previous section). The time period between the end of the hydrogen charging operation and the beginning of the TDS measurement is about 75 minutes. This time includes the specimen preparation (the removal of the oxide layer that was formed during the charging step) and a pumping time (around 60 minutes) to reach a high vacuum ($\approx 10^{-7}$ mbar) in the TDS instrument. Meanwhile, a part of the hydrogen called "diffusible hydrogen" had escaped from the sample due to its high mobility [26]. This feature must be taken into consideration when interpreting TDS data.

The TDS instrument used in this study was calibrated using commercial hydrogen standards (titanium pins and steel pins) purchased from LECO France. Titanium standards have an average mass of 0.12 g and a certified hydrogen concentration of 103 ± 7 wt ppm, which represent a hydrogen mass of 1.24×10^{-5} g, whereas steel standards have a nominal mass of 1 g and a hydrogen concentration of 8.1 ± 0.8 wt ppm which corresponds to a hydrogen mass of 0.81×10^{-5} g.

To evaluate the real hydrogen content in the calibration standards and in the TDS samples of G20MN5 steel, the spurious effect of water adsorbed at the samples surfaces was thoroughly investigated (the results are not presented in this document). This problem has been reported in several TDS studies [37][38][39] and the authors concluded that peaks of hydrogen, related to the dissociation of adsorbed water on the sample surfaces, start to appear after exposing

the sample to the atmosphere even for a short period [38][39]. In our calibration procedure, the TDS signal of the hydrogen coming from adsorbed water, although small, was subtracted from the genuine hydrogen TDS signal of the calibration standard. For the TDS samples of G20MN5 steel, no hydrogen peak related to the dissociation of adsorbed water on the sample surfaces was found below 550°C (as it can be seen in Figure 10, no peak of hydrogen was found in the case of the non charged sample). In our case, hydrogen peaks coming from adsorbed water appear only beyond 550°C. The TDS measurements presented in this work were limited to a temperature of 500°C in order to avoid spurious peaks related to adsorbed water on the sample surfaces.

III Results and discussions

III.1 Material characterization

III.1.1 Porosity characterization

A forged sample and a cast sample were scanned using X-ray tomography in order to characterize the porosity. The same thresholding was applied on all the samples in order to identify the voids inside the material. Figure 1 (a) and (b) present cross section images of a cast sample and a forged sample respectively. The absence of porosity has been established for the forged sample studied here, whereas, the presence of cavities in the cast sample is clearly evidenced.
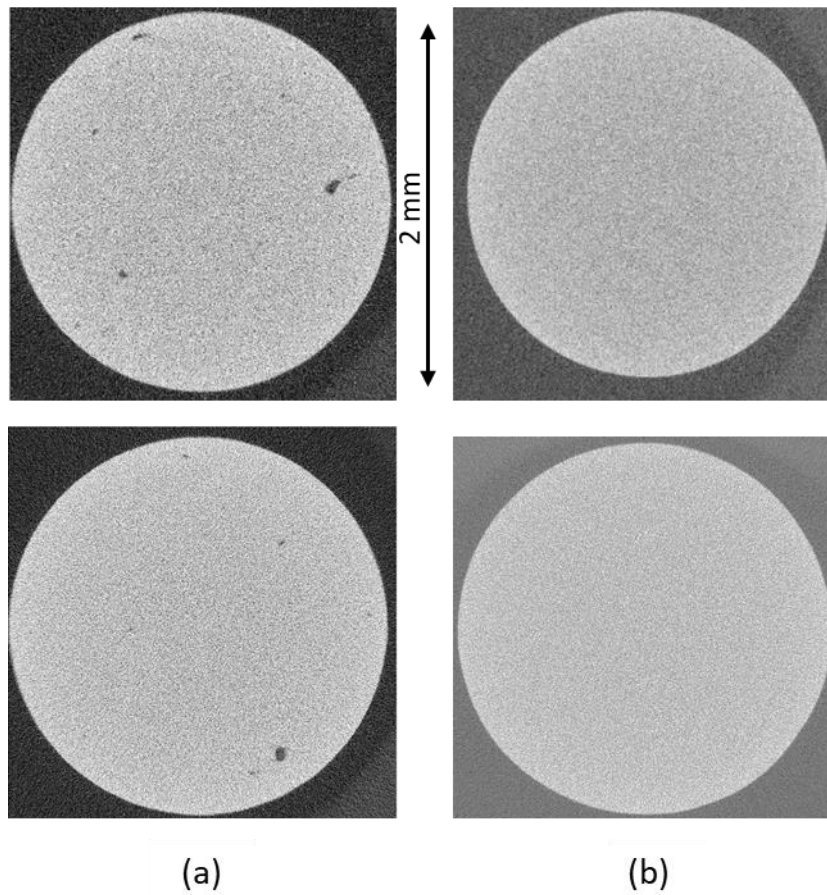
Figure 1 : Cross sectional views of (a) a cast sample (b) a forged sample based on X-ray tomography data, showing a few cavities in the cast sample and the absence of porosity in the forged sample.

The X-ray reconstructed volume for the cast sample is presented in Figure 2. It shows clearly the presence of cavities (blue particles). In general, it appears that the cavities are evenly distributed over the sample. However, the size and the shape are different from one pore to another. This 3D volume reconstruction is a very useful tool to obtain relevant statistical information on the porosity inside the sample.
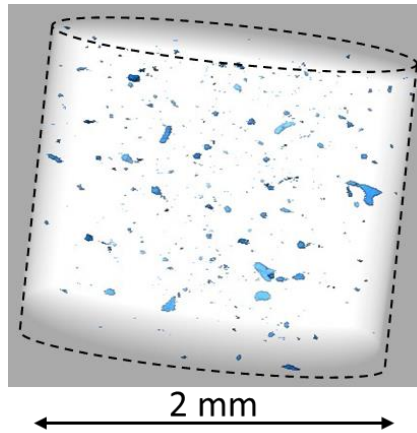
Figure 2 : 3D volume rendering of a cylindrical cast sample (diameter = 2 mm) based on X-ray tomography, showing the distribution of the cavities.

This 3D volume was investigated in order to quantify and to characterize the porosity in the cast material. Figure 3 shows the distribution of porosities based on their equivalent diameter. The equivalent diameter of a particle is defined as the diameter of a sphere that has the same volume as the measured particle. The histogram shows that the majority of cavities (nearly 96%) have an equivalent diameter inferior to 20 µm and that the maximum equivalent diameter is equal to 68 µm. Table 2 gives additional information on the porosity features. In this specimen, the average equivalent diameter of cavities is 7.6 µm and the volume of voids represents 0.05 % of the total volume of the sample.
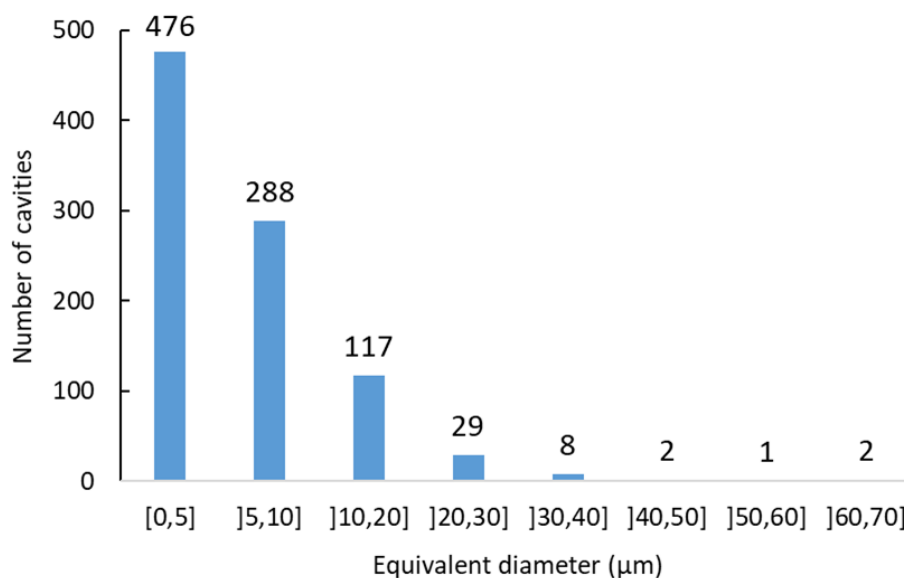

Figure 3 : The distribution of the cavities based on their equivalent diameter obtained from X-ray tomography. Most of cavities have an equivalent diameter inferior to 20 µm.

Table 2 : Porosity features in a cast sample obtained using X-ray tomography.

Total number of cavities	Average equivalent diameter (μm)	Cavity density (μm⁻³)	Inter-cavity distance (μm)	Porosity fraction (%)
923	7.6	3.8×10^{-7}	138	0.05

In this work, it was not possible to obtain the porosity fraction of EP samples (26x20x1.9 mm) and TDS samples (11x26x1.9 mm) by X-tomography scans because of constraints on the specimens' size and shape. Therefore, the hydrostatic weighing technique was used to determine the porosity volume fraction for EP and TDS specimens.

The reference density was that of the forged material as it was shown earlier that this material has no porosity. The cast samples were taken from different zones in the ingot in order to have different porosity fraction from one sample to another. Table 3 summarizes the results of the hydrostatic weighing technique performed on the cast samples. The uncertainty of these results is around ±0.02%.

Table 3 : The volume fraction of porosity for different cast samples determined by the hydrostatic weighing technique

	EP samples		TDS samples				
	1	2	1	2	3	4	5
Volume fraction of porosity (%)	0.04	0.07	0.13	0.18	0.20	0.25	0.27

III.1.2 Microstructural characterization

As mentioned above, the cast and forged bars were normalized at 880°C for 60 minutes. Forged and cast samples were ground and polished to 1 μm, then they were etched using a 5% Nital solution (ethanol + nitric acid). Figure 4 (a) and (b) present optical micrographs of the cast and forged materials respectively. A typical ferrite – pearlite microstructure is observed in both cases. Several metallographic observations, at different places of the samples, showed a similar microstructure in both materials. The pearlite fraction and ferrite grain size were

determined on the different micrographs using ImageJ software. The pearlite fraction is equal to 29±2 % and 32±3 % for the cast material and the forged material respectively. The ferrite grain size is 12.6±1.2 μm for the cast sample and 11.6±1.0 μm for the forged sample. Thus, very small difference in pearlite fraction and grain size is obtained between the two materials. Such a small difference is not expected to affect hydrogen diffusion significantly. We inferred that, if a significant difference in hydrogen behavior is found between a forged sample and a cast sample, it should be related to a difference in porosity, not in microstructure.
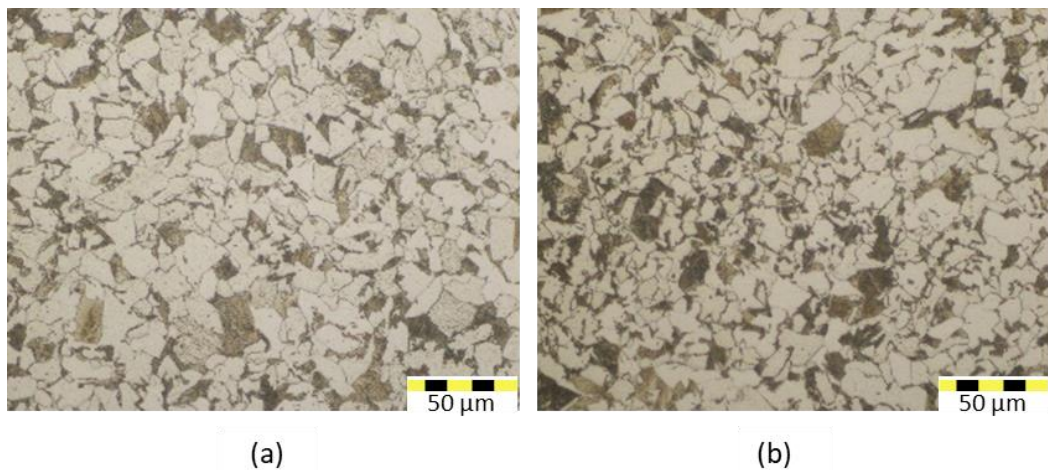

Figure 4 : Optical micrographs of etched (a) cast sample and (b) forged sample showing a ferritic-pearlitic microstructure. The micrographs were taken from regions of the specimen showing no porosity.

III.2 Hydrogen electrochemical permeation

The permeation experiments were performed at room temperature. Three samples (1 forged sample + 2 cast samples) have been tested under the same conditions. Hydrogen permeation results are expressed in normalized current density (J/J_{max}, with J_{max} the steady state-current), as a function of the normalized time (t/e^2, with t the time in seconds and e the specimen thickness in meter). This normalization was made to remove the dependence of results on sample thickness. The values of the current density at the steady state (J_{max}) are displayed in Table 4.

Table 4 : Samples characteristics and hydrogen permeation results. J_{max} is the hydrogen flux at the steady state, $J_{max\ desorption}$ is the hydrogen flux at the end of the charging step, D_{eff} is the effective diffusion coefficient calculated using the time-lag method based on the flux of the final steady state and D_1 is the effective diffusion coefficient calculated using the time-lag method based on the flux of the pseudo-steady state (see text).

Sample	Charging					Desorption
	Porosity fraction (%)	Thickness (mm)	J_{max} (nA/cm²)	D_{eff} (m²/s)	D_1 (m²/s)	$J_{max\ desorption}$ (nA/cm²)
Forged	0	1.96	1220	7.8×10^{-12}	2.4×10^{-10}	1190
Cast 1	0.07 ± 0.02	1.96	1180	3.3×10^{-12}	2.5×10^{-10}	1090
Cast 2	0.04 ± 0.02	1.83	1375	3.7×10^{-12}	2.4×10^{-10}	1230

Liu et al. studied the influence of the microstructure on hydrogen permeation and trapping in steels [40]. The materials used in their study were pure iron and two ferritic-pearlitic steels (AISI 1018 and AISI 4340) that have a similar chemical composition and a similar microstructure to our material. The results of their study revealed that there are mainly two types of trapping sites. The first type include ferrite grain boundaries and dislocations and the second type corresponds to the ferrite-cementite interfaces. Thus, we assume that our material should contain the same trapping sites due to the close similarity of the microstructures and the chemical compositions.

The aim of this section is to compare the hydrogen permeation results between the forged and the cast samples to reveal the role of porosity in the hydrogen trapping and diffusion phenomena. As explained earlier, the only difference between the samples was the porosity. Therefore, if any significant variation in the permeation behavior will occur, it is beyond all doubt due to the cavities.

Figure 5 (a) and (b) present the permeation rising transients for the three samples. It is to be mentioned that for two of the presented curves, a slight drop of the steady state current is observed. This might be the result of a slight variation of the exit surface state during the experiment. For this reason, the absolute values of the diffusion coefficients determined later might be considered with caution, as the uncertainty might be significant. However, comparison is possible and the results show that the forged sample reaches the steady state faster than the two cast samples. The effective diffusion coefficients were calculated using the

time-lag method (Eq.1). The diffusion coefficient obtained is equal to 7.8×10^{-12} m²/s for the forged sample, 3.7×10^{-12} m²/s for the cast sample with a porosity fraction of 0.04% and 3.3×10^{-12} m²/s for the cast sample with a porosity fraction of 0.07%. In general, the decrease in hydrogen mobility is linked to the trapping sites because they absorb hydrogen, which leads to the decrease of the diffusion rate. In our case, the only difference between the forged sample and the cast samples is the porosity thus, it is clear that cavities act as hydrogen traps. We assume that the delay to reach the steady state for the cast samples compared to the forged sample corresponds to the time needed to fill the cavities with hydrogen in order to reach local equilibrium. This equilibrium is described by Sieverts' law which indicates that the lattice hydrogen concentration at a given depth of the permeation specimen is proportional to the square root of the pressure inside the cavity or more precisely proportional to the square root of the fugacity [41]. It is then expected that, in the steady state, the amount of hydrogen stored in the cavities is proportional to the porosity fraction, which implies that the time needed to reach steady state should increase with increasing porosity fraction. As it can be seen also from Figure 5 (a), the permeation curve of the cast sample with a porosity fraction of 0.07% shows a shoulder around 3×10^{10} s/m². We assume that this shoulder could be related to the distribution of cavities along the thickness of the sample, but this possibility was not investigated in depth in the present study. The hydrogen effective diffusion coefficient (obtained using the 63% time-lag method) of the two cast samples is practically the same (3.7×10^{-12} m²/s and 3.3×10^{-12} m²/s), although there is almost a factor of two between their respective porosity fraction. However, it should be reminded that the uncertainty on the porosity fraction is relatively high (± 0.02%), so the actual difference between the two fractions measured may be less than a factor of two.

Figure 5 (a) shows a closer view of the beginning of the permeation curves. It is remarkable that the permeation curves obtained in this study show a double regime rising transient. At the beginning (see Figure 5 (b)), there is no hydrogen flux (current density) at the exit side, then, when hydrogen atoms reach the detection side, a first rise is observed. It is noticeable that for the three samples, the hydrogen flux starts to rise approximately at the same moment ($t/e^2 \approx 3 \times 10^8$ s/m²). Then, well before reaching the final steady state, a pseudo-steady state is reached for the three samples at about $t/e^2 \approx 1.5 \times 10^9$ s/m². Then, for $t/e^2 > 10^{10}$ s/m², the hydrogen flux starts to rise again until reaching the final steady-state. It is remarkable that the

existence of this pseudo steady-state is not related to porosity as it exists in the forged specimen. It is thus inferred that it is related to the microstructure of the material, not to porosity.

The effective diffusion coefficients were calculated for the first transient using the time-lag method. We found approximately the same value in the three experiments ($D_1 = 2.4 \times 10^{-10}$ m²/s), which is higher by about two orders of magnitude than the diffusion coefficients determined previously, ranging from 3.3 to 7.8×10^{-12} m²/s. This shows that part of the hydrogen was able to diffuse across the specimen by following fast diffusion paths. Most probably, hydrogen diffused through the percolated ferrite corridors, without interacting too much with the porosities and/or the pearlite where hydrogen mobility can be affected [42] (because of the high trapping energy of the interfaces in pearlite, which is about 65 kJ/mol [43][44]). However, a detailed description of this mechanism would require more research and it is beyond the scope of this work that focuses on the effect of porosities.
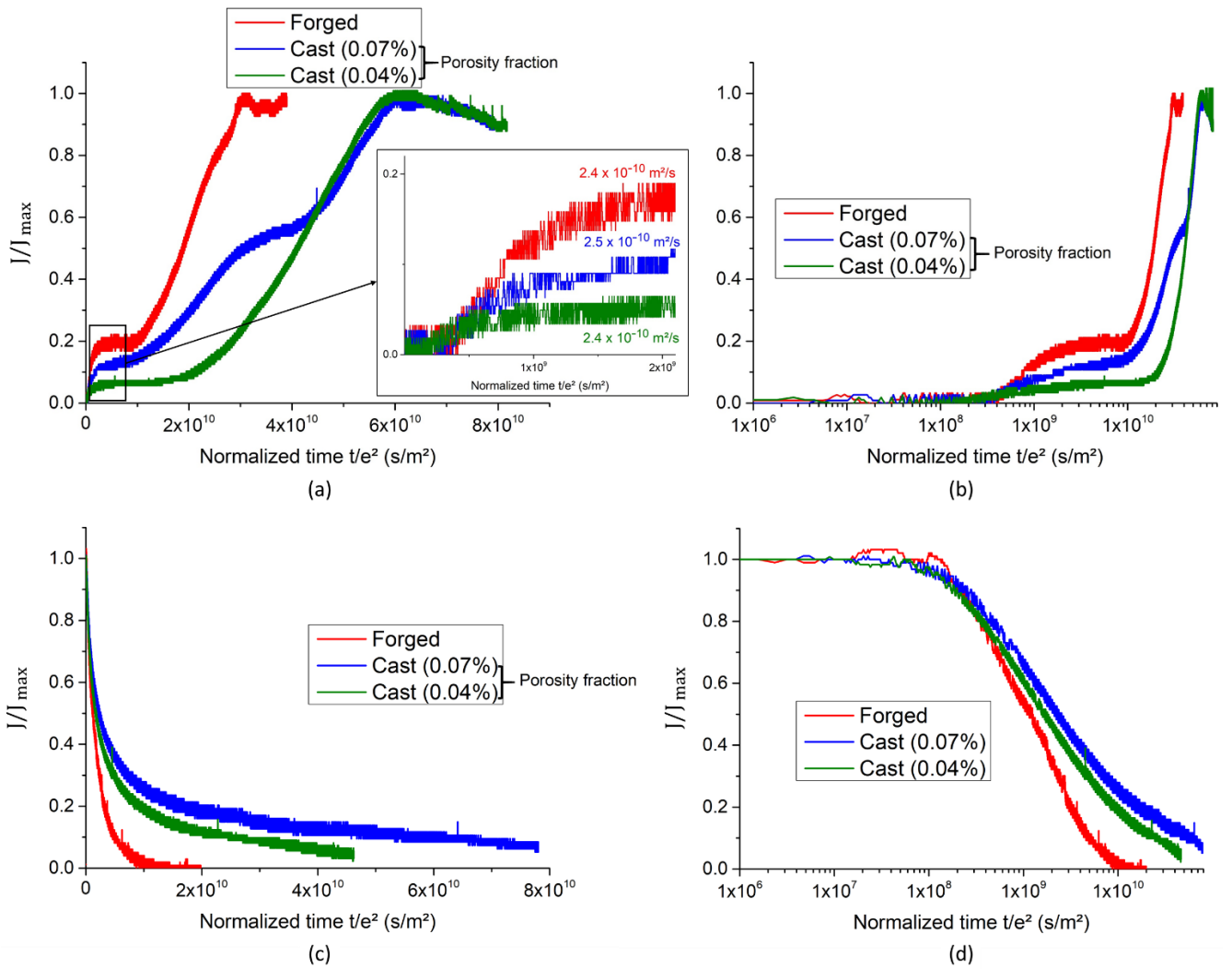
Figure 5 : Electrochemical hydrogen permeation results for a forged sample (red curve), a cast sample with a porosity fraction of 0.07% (blue curve) and a cast sample with a porosity fraction of 0.04% (green curve). Permeation experiments were performed under the same conditions in a 0.1M NaOH aqueous solution at room temperature. (a) and (b) normalized rising transient, (c) and (d) normalized decaying transient.

The effect of the porosity is also very clear during the decaying transient as illustrated in Figure 5 (c) and (d). The area under each curve reflects the quantity of hydrogen that desorbed through the detection side. Comparing the decaying transients, a significant difference in the amount of desorbed hydrogen can be noticed between the forged sample and the cast samples. Since the main distinction between the samples is the porosity, this difference in the desorbed hydrogen can only correspond to the hydrogen stored in the porosity. In addition, the comparison between the two cast samples shows that the amount of the desorbed hydrogen from the sample with a porosity fraction of 0.07% is higher than that of the cast sample with a porosity fraction of 0.04%. This suggests that the amount of absorbed hydrogen increases with increasing porosity fraction.

The hydrogen that desorbs at room temperature during the permeation decaying transient is a combination of lattice hydrogen and reversibly trapped hydrogen. The irreversibly trapped hydrogen, if any, could not desorb at room temperature. Consequently, it is safe to conclude that the porosity acts as a reversible trap for hydrogen at room temperature.

Figure 6 shows the decay transients for the forged sample and the cast sample with a porosity fraction of 0.07%. The hatched area (area between the two curves) represents the difference in the amount of desorbed hydrogen between the cast sample and the forged sample, which is the hydrogen trapped in the porosity. This hydrogen is about 85% of the total amount of the desorbed hydrogen from the cast sample. It should be noted that this percentage is probably underestimated, as the decaying transient of the cast specimen had not reached zero yet when the experiment was stopped.

To sum up, EP results showed that porosity plays an important role in hydrogen trapping and diffusion. The rising transients indicate that hydrogen diffusion rate is lower in the case of the cast samples compared to a sample without porosity. The decaying transients proved that the majority of hydrogen is located at the porosity and that this porosity acts as a reversible trap for hydrogen.
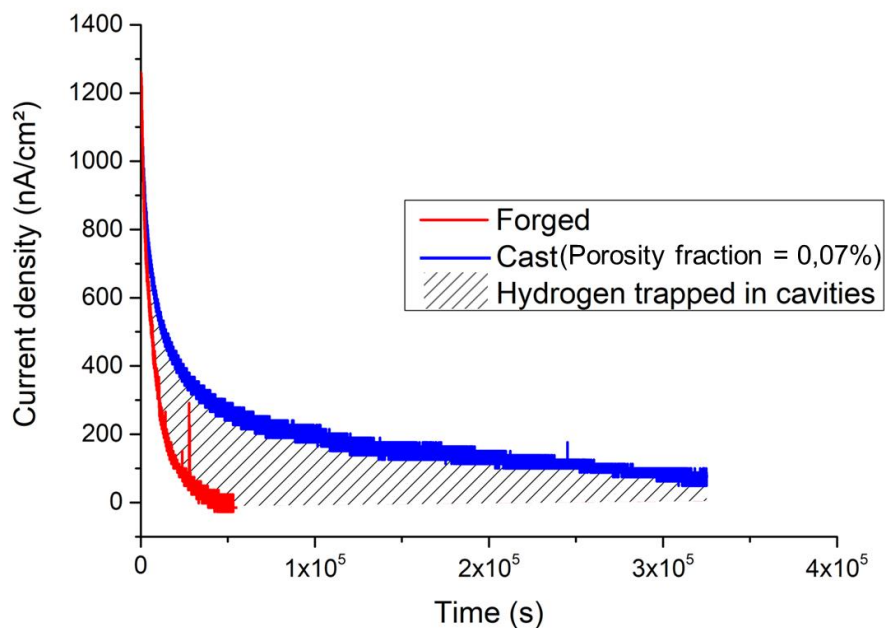

Figure 6 : Decay transients for the forged sample (red curve) and the cast sample with a porosity fraction of 0.07% (blue curve).The area between the two curves represents the hydrogen trapped in the porosity. It corresponds to 85% of the total desorbed hydrogen.

III.3 Chemical charging operation

The chemical charging temperature (50°C) was chosen to increase the hydrogen mobility and consequently decrease the charging time compared to charging at 20°C. In order to estimate the effective diffusion coefficients at 50°C, we used the diffusion coefficients from our permeation tests (presented in the previous section, these tests were performed at 20°C) and data from J.G Sezgin et al. [11] and Husby at al. [45]. In their studies, they were able to obtain values of hydrogen diffusion coefficient at different temperatures for a material similar to ours. First, using the data from Sezgin et al., we calculated the ratio between the diffusion coefficients at 50°C and at 20°C ($D_{50°C}/D_{20°C}$). Similarly, using the data from Husby et al., we calculated the ratio between the diffusion coefficients at 45°C and at 15°C. We found that these ratios ranged between 1.9 and 2.6. Finally, we multiplied our diffusion coefficients, obtained from permeation at room temperature, by a factor of 2 in order to obtain an estimation of our effective diffusion coefficients at 50°C. The results are presented in Table 5. For the cast material, a diffusion coefficient of 3.3×10^{-12} m²/s at room temperature was considered here.

Table 5: The effective diffusion coefficients obtained by the time-lag method based on electrochemical permeation tests and the estimated values of these coefficients at 50°C.

D_{eff}[m^2/s]	Forged	Cast
at 20°C (permeation test)	7.8×10^{-12}	3.3×10^{-12}
at 50°C (estimation)	1.6×10^{-11}	6.6×10^{-12}

Numerical simulations of hydrogen charging were performed using the estimated diffusion coefficients at 50°C. Figure 7 (a) and (b) present the time-dependence of the concentration profiles for a cast sample and a forged sample respectively. For a forged sample, 24 h of charging should be enough to reach a homogenous concentration inside the sample, within 98%. However, for a cast sample, it appears that after 24 h the hydrogen distribution is not homogenous (the average concentration inside the sample is about 83% of the subsurface concentration after 24 h and it is 95% after 40 h). It should be mentioned however that the simulated concentration profile is only an approximation as the diffusion coefficient used in the simulation is not accurately known. Indeed this effective diffusion coefficient is expected

to depend on the porosity fraction, which can significantly vary from one specimen to another, as shown later.

Increasing the charging time would certainly ensure a more homogeneous hydrogen distribution inside the sample but for practical reasons we limited the charging time to 24 h. The effect of the charging time on hydrogen content will be discussed later. Another way to ensure a more homogenous hydrogen distribution is by decreasing the specimen thickness. Unfortunately, this solution is not recommended in our study because this decrease will lead to a much higher uncertainty in the determination of the volume fraction of porosity.
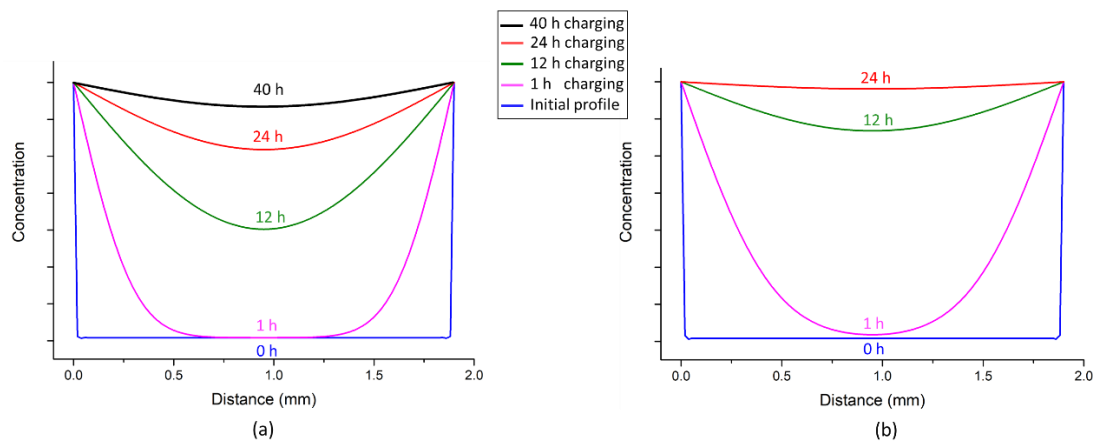

Figure 7 : Concentration profiles of hydrogen at various times estimated by numerical simulation of the charging operation at 50°C. The thickness, in both simulations, is 1.9 mm. (a) cast sample with an effective diffusion coefficient of 6.6×10^{-12} m²/s. (b) forged sample with an effective diffusion coefficient of 1.6×10^{-11} m²/s.

III.4 Hydrogen Thermal Desorption Spectroscopy

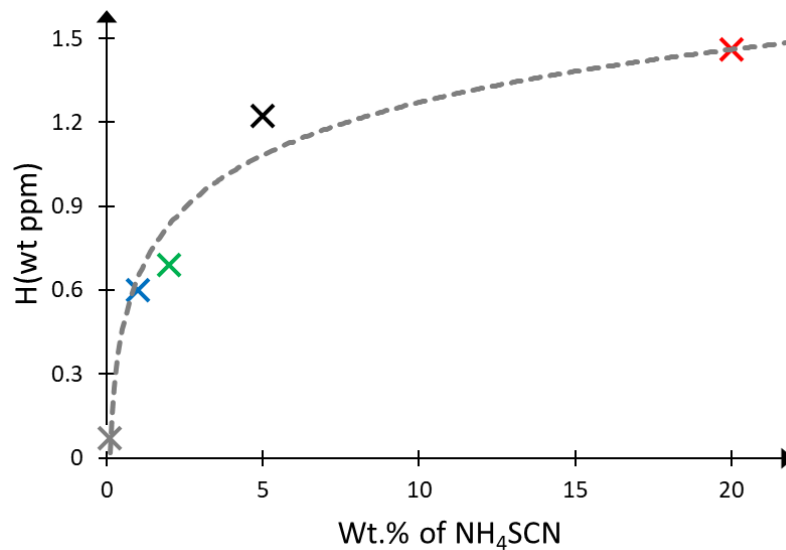## III.4.1 Solution concentration and hydrogen content

In order to highlight the effect of the NH_4SCN concentration of the charging solution on the amount of hydrogen absorbed in the material, the same cast sample was analyzed by TDS several times. At each time, the sample was immersed in an aqueous solution with a specific mass concentration of NH_4SCN (0%, 1%, 2%, 5% and 20%) for 24 h. The solution was continuously heated at 50°C. Then, the TDS measurements were performed with a heating rate of 10°C/min up to 500°C. After the last measurement, the microstructure was investigated under optical microscope to ensure that the repetitive heating to 500°C had no impact on the microstructure.

The desorption spectra for the different NH_4SCN concentrations are shown in Figure 8 (a). The hydrogen concentrations indicated in the legend were obtained by integration of each curve. These results indicate that the amount of hydrogen absorbed in the material increases when the NH_4SCN solution concentration is increased. For instance, with the increase of the NH_4SCN mass fraction from 1% to 5%, the hydrogen content has doubled from 0.60 wt ppm to 1.22 wt ppm. A similar trend was found by Takagi et al.[46]. Figure 8 (b) presents the influence of the NH_4SCN concentration on the hydrogen content. The hydrogen content is plateauing for NH_4SCN concentrations above 5%: the increase in hydrogen content is of 0.24 wt ppm (19%) only when the NH_4SCN concentration is increased from 5 wt% to 20 wt%.

Finally, a hydrogen peak is clearly evidenced on the TDS spectrum after immersion in pure water, which corresponds to a hydrogen content of 0.07 wt ppm. It is assumed that corrosion reactions take place even in pure water at the specimen surface, which results in hydrogen absorption.
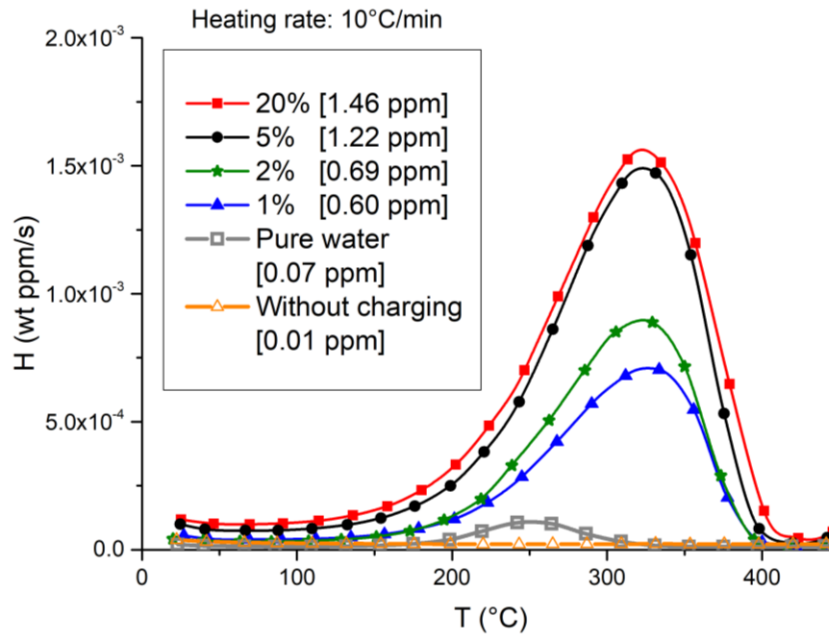
Figure 8 : The effect of the NH4SCN solution concentration on the hydrogen content for a cast sample after 24h of immersion (a) TDS spectra; heating rate = 10°C/min (b) Hydrogen content as a function of the charging solution concentration. The hydrogen content was evaluated from TDS peak integration. The same sample was used for all the experiments.

III.4.2 Charging time and hydrogen content

The aim of this section is to investigate the influence of the charging time on hydrogen content. Four charging operations were performed on the same cast sample and after each charging operation the hydrogen content was measured using TDS. Charging was conducted in a NH4SCN aqueous solution heated at 50°C for two different durations and two NH4SCN

concentrations. Figure 9 (a) shows the TDS results (heating rate 10°C/min) for the four charging conditions. The hydrogen content increases with increasing the solution concentration as explained earlier for both charging times. Figure 9 (b) illustrates the evolution of the amount of absorbed hydrogen as a function of the charging time. For both concentrations, the increase of hydrogen content from 24 h to 40 h of charging is relatively small, especially for the 5 wt% solution where the difference is only 0.15 wt ppm, which represents 12% of increase. This increase is similar to what has been obtained earlier by numerical simulations (see Figure 7). The numerical results showed an increase of 14% between 24 h and 40 h of charging.

To sum up, since 40 h of charging, for both solution concentrations, do not increase significantly the final hydrogen content, 24 h of charging were considered more adequate.
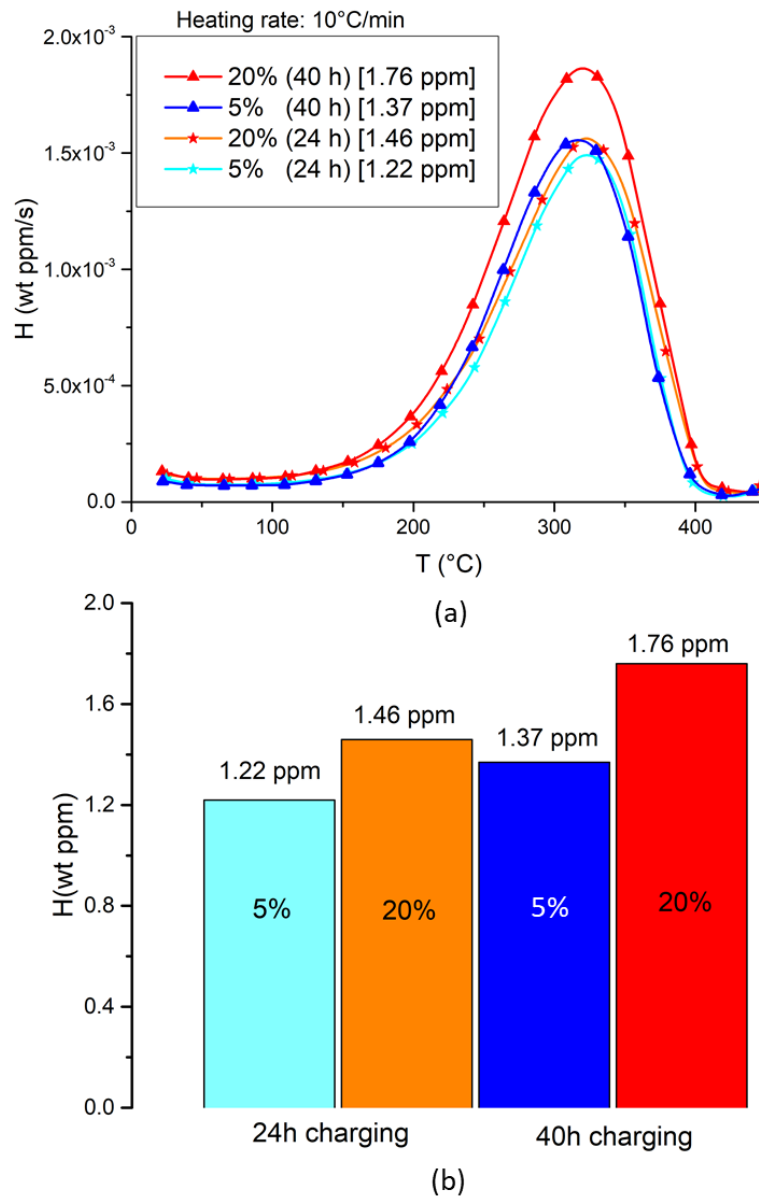
Figure 9 : The influence of the immersion time on the amount of absorbed hydrogen for two different NH₄SCN concentrations (5 wt% solution and 20 wt% solution**)** (a) TDS spectrums; heating rate = 10°C/min (b) Hydrogen content as a function of the charging solution concentration. The hydrogen content was evaluated from TDS peak integration. The same sample was used for all the experiments.

III.4.3 The role of porosity in the hydrogen trapping process

In order to investigate the role of porosity in the hydrogen trapping process, two samples were chemically charged for 24 h under the same conditions as described earlier. The first sample was a cast one (thickness = 1.82 mm) with a volume fraction of porosity of 0.27%. The second was a forged sample (thickness = 1.85 mm). After charging, TDS measurements were performed with a heating rate of 10°C/min up to 500°C. The results are presented in Figure 10. An additional non-charged cast specimen was studied as well to ensure the absence of

hydrogen in the initial state (grey curve in Figure 10). When comparing the TDS spectrums, it can be observed from the area under the curve that there is a huge difference in the amount of desorbed hydrogen between the cast and the forged specimens. For the cast sample (blue curve), the desorption peak maximum is located at 320°C and the amount of the desorbed hydrogen is 1.50 wt ppm. For the forged sample (red curve), the peak maximum is at about 250°C and the amount of hydrogen is only 0.16 wt ppm which is very low compared to the cast sample. This significant difference corresponds to the amount of hydrogen trapped in the cavities (hatched area) because, as explained earlier, the only difference between the two samples lies in the porosity. Therefore, it can be concluded that cavities are traps for hydrogen. Furthermore, another interesting conclusion can be made which is that the absorbed hydrogen is essentially located at cavities (90% in this case, calculated by dividing hydrogen content inside the cavities by the total hydrogen content of the cast sample). Finally, these findings confirm the conclusions made earlier based on the permeation tests that indicate that the porosity is a trap for hydrogen and that most of the absorbed hydrogen is in the cavities.
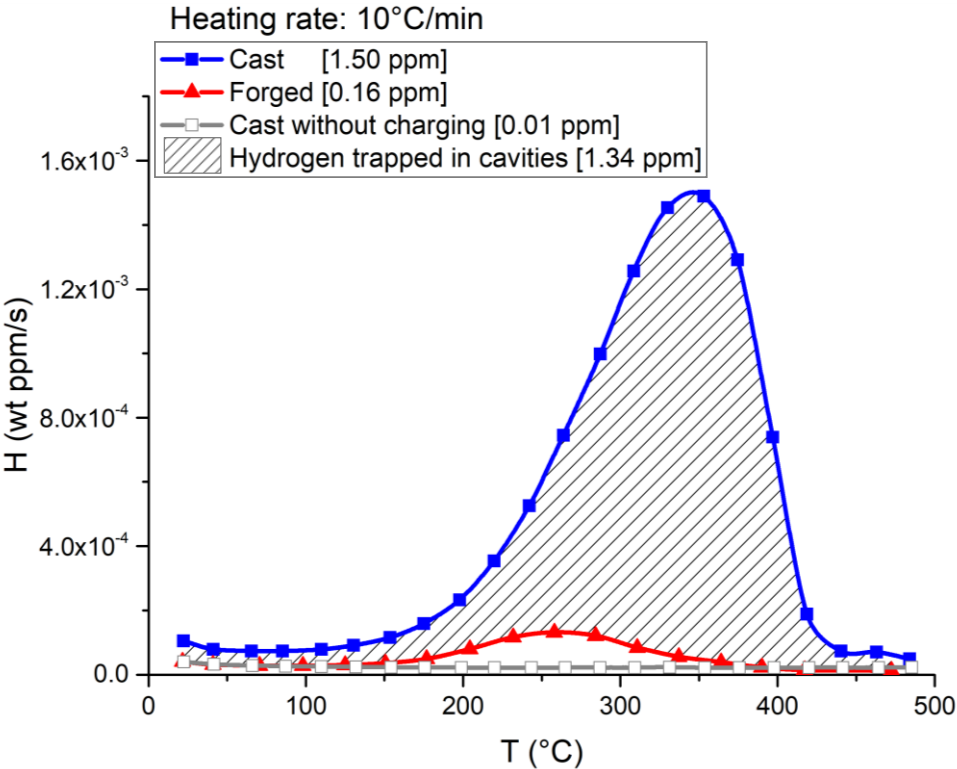

Figure 10 : TDS spectra for a cast sample without charging, a charged cast sample and a charged forged sample. The charging was performed in a 5 wt% NH₄SCN aqueous solution for 24 h charging. The heating rate was 10°C/min. The cast sample has a volume fraction of porosity of 0.27%.

A comment is due here on the state of hydrogen present in cavities. Based on the results of Figure 10, 1.34 wt ppm of hydrogen, obtained by subtracting the concentrations measured in the cast and forged specimens respectively, was trapped in the cavities. Considering the mass of the specimen used (4.3 g), this corresponds to 5.8×10^{-6} moles of H atoms. It can be questioned whether this hydrogen is under the molecular form (gas) and/or under the atomic form adsorbed on the internal surfaces of the cavities. Assuming that the cavities are spherical and they have a diameter of 7.6 μm (based on the X-ray tomography results presented earlier in Table 2), we need 6.38×10^6 cavities in order to achieve the volume fraction of porosity for this sample, which is 0.27%. This represents an internal surface area of 1.16×10^{-3} m². In order to estimate the amount of hydrogen that can be adsorbed on such an area, a hydrogen adsorption site density of 2.85×10^{-5} mol/m² will be considered, which corresponds to that of a (110) surface plane [47]. If all the adsorption sites of the internal surfaces of cavities were occupied, the maximum amount of adsorbed hydrogen would be 3.3×10^{-8} moles. This is inferior to 1% of the total amount of trapped hydrogen in the cavities (5.8×10^{-6} moles). Consequently, this calculation, based on experimental data, demonstrates that the hydrogen is mainly under the gaseous form in this case. In a general way, for a given porosity fraction, the distribution of hydrogen between the adsorbed and gaseous states depends on the size of cavities and the pressure inside them as demonstrated by Wong [48].

To sum up, these measurements permitted to identify the contribution of the porosity in the hydrogen trapping process. It indicates that the porosity acts as trap for hydrogen in which a large amount of hydrogen can be stored. In addition, in our case, this hydrogen is mostly under the molecular form. However, the question that remains is whether the porosity is a reversible or irreversible trap at room temperature. A more detailed discussion is presented in the next section.

III.4.4 Hydrogen desorption at room temperature

Figure 11 (a) summaries TDS measurements that were performed on the same charged cast sample after different times spent at room temperature. The same sample, with a porosity volume fraction of 0.13%, was charged five times under the same conditions (in a 5 wt% NH₄SCN solution at 50°C). After each charging operation, it was stored at room temperature for a certain period before starting the TDS measurement. The analyses were done after 75 minutes, 6 h, 24 h, 3 days and 7 days. The corresponding amounts of hydrogen

extracted from the TDS data are respectively: 1.01 wt ppm, 0.74 wt ppm, 0.42 wt ppm, 0.16 wt ppm and 0.02 wt ppm. The first value represents the hydrogen content 75 minutes after the end of charging, 75 minutes being the minimum time necessary for preparing the specimen and pumping the TDS instrument. The other values represent the amount of hydrogen remaining in the sample after a certain time spent at room temperature. After seven days, TDS data did not show any hydrogen peak up to 500°C. This indicates that the absorbed hydrogen that was measured immediately after charging (red curve) was able to desorb completely from the sample at room temperature. Figure 11 (b) presents the simulated concentration profiles after different times of desorption at room temperature using the effective diffusion coefficient determined by EP for the cast sample ($3.3x10^{-12}$ m²/s). Figure 11 (c) shows the evolution of the remaining hydrogen content as a function of the desorption time at room temperature. The blue dashed curve represents the result of a simulation using the effective diffusion coefficient determined by EP for the cast sample ($3.3x10^{-12}$ m²/s), the cross marks correspond to the TDS measurements. The red dotted curve is the result of a simulation using an adjusted diffusion coefficient ($2.7x10^{-12}$ m²/s) in order to fit best to the experimental data. This adjusted diffusion coefficient is slightly lower than the effective diffusion coefficient obtained by EP, which is expected because the porosity fraction of the TDS sample (0.13 ± 0.02%) is relatively higher than that of the EP sample (0.07± 0.02%). These data indicate that the hydrogen concentration decreases with increasing the desorption time until reaching almost zero after seven days. In conclusion, this absorbed hydrogen was able to quit the sample at room temperature and at the same time, it corresponds mainly to the hydrogen trapped in the cavities as demonstrated in the previous section. Therefore, the porosity can be considered as a reversible trap for hydrogen at room temperature. This conclusion is the same as that found using EP.
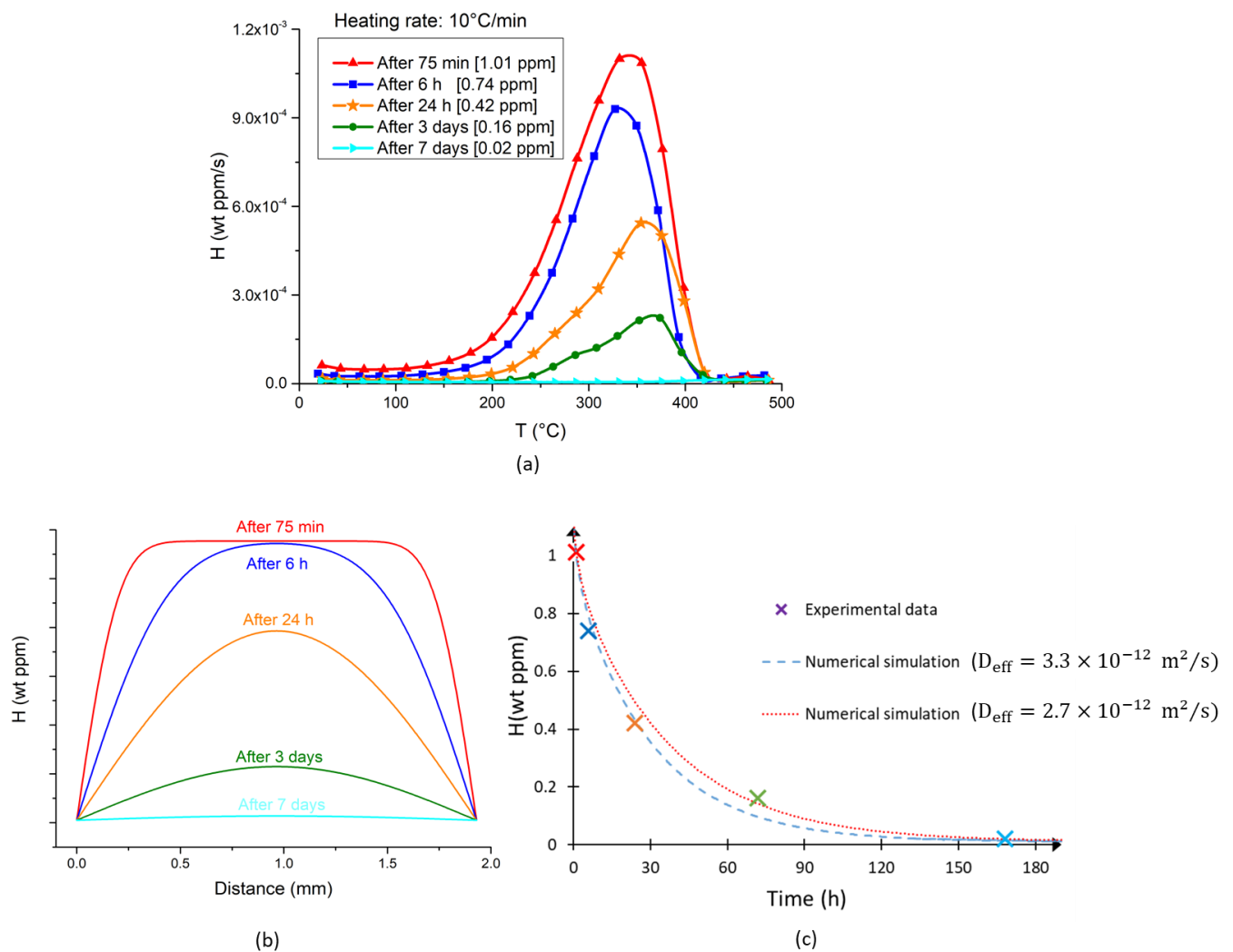
Figure 11 : The effect of the desorption time at room temperature on the hydrogen content for a cast sample (a) TDS spectra after hydrogen charging followed by different times of desorption at room temperature; heating rate = 10°C/min. (b) The evolution of hydrogen concentration profile as a function of time at room temperature based on numerical simulations. (c) Hydrogen content evolution as a function of desorption time. The dashed curve corresponds to the numerical results. The points correspond to hydrogen contents determined from TDS peak integration. The same cast sample (volume fraction of porosity = 0.13%) was used for all the experiments. Charging was performed in a 5 wt% NH$_4$SCN aqueous solution for 24 h.

III.4.5 Hydrogen content and porosity fraction

The aim of this section was to investigate the correlation between the amount of absorbed hydrogen and the volume fraction of porosity. Therefore, one forged sample and five cast samples were used. The cast samples were taken from different zones in the ingot in order to have different porosity fractions from one sample to another. The samples were charged for 24 h in a 5 wt% NH$_4$SCN solution heated at 50°C. Then, TDS measurements were performed with the same heating rate as the previous measurements (10°C/min). Figure 12 (a) shows

hydrogen thermal desorption spectrum for each sample. The desorption peak maximum is around 350°C for the five cast samples and around 230°C for the forged sample. As can be seen, the hydrogen content is different from one sample to another, especially between the forged sample and the cast samples. The amount of absorbed hydrogen increases linearly with increasing porosity fraction as illustrated in Figure 12 (b). This proves, as can be expected, that a higher volume fraction of porosity leads to a larger hydrogen uptake. In fact, if we charged different cast samples in the same conditions, cavities in all the samples should reach the same pressure at equilibrium and a linear relation between porosity fraction and hydrogen content is expected.

It should be mentioned that the hydrogen concentrations presented in Figure 12 include gaseous hydrogen in the cavities, as well as hydrogen "dissolved" in the metal, the latter being about 0.16 wt ppm as measured on the forged specimen. More precisely, this "dissolved" hydrogen most probably corresponds to hydrogen shallowly trapped in the microstructure.
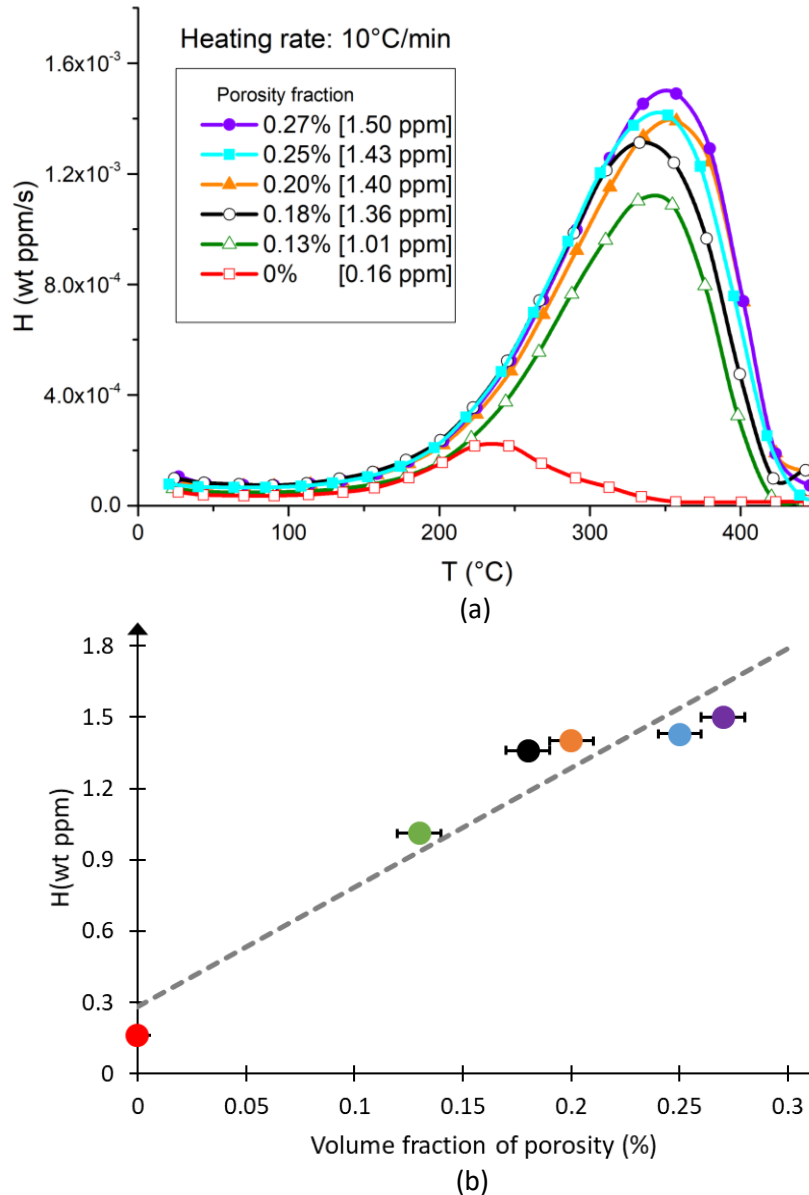
Figure 12 : The relationship between the amount of absorbed hydrogen and the volume fraction of porosity (a) TDS spectra; heating rate = 10°C/min (b) The evolution of hydrogen content as a function of the volume fraction of porosity. The hydrogen content was determined from TDS peak integration. All samples were charged in a 5 wt% NH₄SCN aqueous solution for 24 h. The error bars represent an uncertainty of 0.02% for the volume fraction of porosity.

III.5 Determination of hydrogen fugacity and solubility

In the following, a method is proposed to determine hydrogen fugacity and hydrogen solubility (Sieverts constant) in the studied material. Table 6 shows the hydrogen concentration measured using TDS in five cast specimens with different porosity fractions. A correction factor of 1.16 was applied to take account of the hydrogen loss during the period between the end of charging and the beginning of the TDS measurement (approximatively 75

minutes). This correction factor was obtained using numerical simulation of hydrogen desorption at room temperature (with D_{eff} = 3.3x10^{-12} m²/s) for 75 minutes. For each specimen, the concentration of hydrogen inside the cavities can be easily obtained from the difference between the total hydrogen concentration and the concentration of hydrogen dissolved in the metal, that is known from the TDS measurement conducted on the forged material containing no porosity (it is equal to 0.2 wt ppm after correction using a D_{eff} = 7.8x10^{-12} m²/s for the numerical simulation of desorption at room temperature for 75 minutes).

Knowing the void volume and the hydrogen amount inside the cavities for each sample, the pressure can be calculated using Eq.2. This expression is based on Abel-Noble equation of state.

$$P = \frac{n_cRT}{2(V - n_cb)} \qquad (2)$$

with P is the pressure (Pa), n_c represents the amount of atomic hydrogen inside the cavities (mol), R is the universal gas constant (8.31477 J.mol^{-1} K^{-1}), T is the temperature (K), V is the void volume (m³) and b is a constant (1.4598x10^{-5} m³/mol [9]). The fugacity was then evaluated using Eq.3 [49], which represents the relationship between the fugacity and the pressure for an Abel-Noble gas. The hydrogen pressure and fugacity obtained in the different specimens are shown in Table 6

$$\mathbf{f = P\exp\left(\frac{Pb}{RT}\right)} \qquad (3)$$

Table 6 : Hydrogen contents, hydrogen pressure and fugacity in the cavities calculated from Abel-Noble equations for five cast samples with different volume fractions of porosity

Volume fraction of porosity (%)	0.27	0.25	0.20	0.18	0.13
Hydrogen content (wt ppm)	1.50	1.43	1.40	1.36	1.01
Hydrogen content after correction (wt ppm)	1.74	1.66	1.62	1.57	1.18
Pressure (bar)	62	64	78	84	83
Fugacity (bar)	65	66	82	88	87

Figure 13 shows the fugacity obtained in the five different samples as a function of the volume fraction of porosity. For the three specimens with a porosity fraction not higher than 0.2%, similar values of hydrogen fugacity are obtained (85 ± 3 bar). On the other hand, fugacities measured for the two specimens with the highest porosity fractions are significantly lower (65-66 bar). However, as the samples were all charged in the same conditions, hydrogen fugacity should be the same at equilibrium. This decrease in fugacity for the highest porosity fractions can be associated to the non-equilibrium state of the hydrogen inside the samples. It is clear that the samples with a higher void volume need more hydrogen to reach the same pressure (fugacity) as the samples with smaller void volume. Consequently, the charging time, for the samples with higher void volume, should be superior to the others in order to reach equilibrium. The charging time used in this study (24 h) was apparently not long enough for the specimens with the highest porosity fractions. On this basis, we will keep the fugacity value of 85 ± 3 bar obtained using only the three specimens with the lowest porosity fractions. This fugacity can also be considered as the equivalent hydrogen fugacity of the charging environment (5 wt % NH4SCN aqueous solution at 50°C).
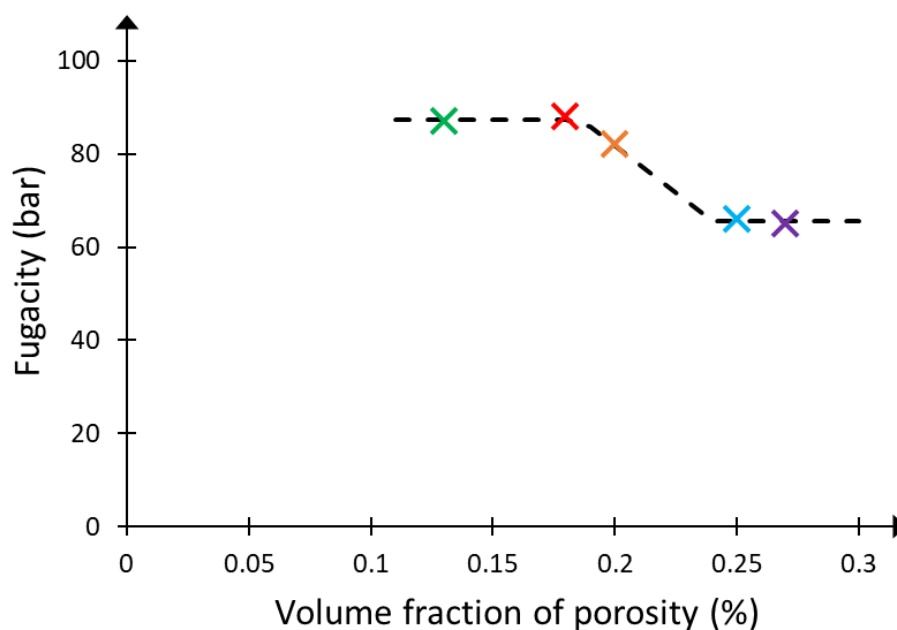

Figure 13 : The plot of hydrogen fugacity as a function of the volume fraction of porosity. The fugacity values were calculated based on the equation of Abel-Noble

The equilibrium between hydrogen dissolved in the metal and gaseous hydrogen in the cavities can be described by the Sieverts' law [50]:

$$C_H = S \sqrt{f_{H_2}} \qquad (4)$$

where C_H represents the concentration of atomic hydrogen dissolved in the material, *S* is the Sieverts constant (hydrogen solubility) and f_{H_2} is the fugacity of gaseous hydrogen in cavities. The Sieverts' law can be obtained by equating the chemical potential of hydrogen dissolved in the metal and that of the gaseous hydrogen in cavities. As shown in Appendix, it is possible to include in the C_H term, not only interstitial hydrogen, but also trapped hydrogen, provided that the trap occupancy is low. It is assumed here that this C_H term in Eq.4 corresponds to the hydrogen concentration measured using TDS in the forged specimen (0.2 wt ppm after correction). As the hydrogen fugacity is known from the analysis shown previously (85 bar), the Sieverts constant of the steel can be determined from Eq.4. It should be mentioned that this value applies at 50°C, which is the hydrogen charging temperature chosen in this study. The value obtained (Eq.5) is in good agreement with that obtained by Sezgin et al. on a similar material [11].

$$\mathbf{S = 2.2 \times 10^{-2} \ wt \ ppm. \ bar^{-1/2}} \qquad (5)$$

IV Conclusions

In this work, the influence of porosity in the hydrogen diffusion and trapping processes has been studied for a low-alloy cast steel by means of electrochemical permeation and thermal desorption spectroscopy. Material characterization showed that the only difference between the forged material and the cast material lies in the porosity. The hydrogen was chemically introduced in thermal desorption spectrometry samples using a NH_4SCN aqueous solution heated at 50°C.

In summary, the most significant findings of this study are:

- Electrochemical permeation experiments showed that hydrogen diffusion in the cast samples was slower than in the forged sample. This is due to the porosity, which acts as trap sites that delay hydrogen diffusion.

- The comparison of the decay transients between the forged and the cast samples showed a significant effect of porosity in the trapping process: the majority of

hydrogen (over 85% of the total desorbed hydrogen) was located in cavities. The same conclusion was found based on thermal desorption spectrometry results.

- Hydrogen was present in cavities as gaseous hydrogen. Hydrogen adsorbed on internal surfaces of cavities was shown negligible.

- Electrochemical permeation and thermal desorption spectrometry experiments have clearly shown that the hydrogen trapped in cavities desorbed spontaneously at room temperature, over some tens of hours for thicknesses of about two millimeters. This proves that the porosity acts as reversible traps for hydrogen at room temperature.

- Thermal desorption spectrometry measurements, performed on samples with different volume fraction of porosity, indicate that hydrogen concentration increased linearly with the increase of the volume fraction of porosity.

- A method was proposed to determine hydrogen fugacity and solubility (Sieverts' constant of the steel) from thermal desorption spectrometry data. In the hydrogen charging conditions used before thermal desorption spectrometry, the hydrogen fugacity and solubility were estimated to 85 bar and 2.2×10^{-2} wt ppm.bar$^{-1/2}$ respectively.

V   Appendix

The chemical potential of lattice hydrogen is

$$\mu_L = \mu_L^0 + RT \ln \frac{\theta_L}{1 - \theta_L} \tag{6}$$

where μ_L^0 is the chemical potential of lattice hydrogen in a reference state and θ_L represents the occupancy of lattice sites, $\theta_L = C_L/N_L$ where C_L is the volume concentration of lattice hydrogen (m^{-3}) and N_L is the number of lattice sites per unit volume (m^{-3}). It is possible also to define the chemical potential of molecular hydrogen inside the voids

$$\mu_{H_2} = \mu_{H_2}^0 + RT \ln f_{H_2} \tag{7}$$

where $\mu_{H_2}^0$ is the chemical potential of molecular hydrogen in a reference state and f_{H_2} is the fugacity of molecular hydrogen. At equilibrium, the chemical potential of hydrogen in lattice sites is equal to the chemical potential of hydrogen in the voids

$$\mu_L^0 + RT \ln \frac{\theta_L}{1 - \theta_L} = \frac{1}{2}\mu_{H_2}^0 + \frac{1}{2}RT \ln f_{H_2} \qquad (8)$$

and since the occupancy of lattice sites is very low ($\theta_L \ll 1$), Eq.8 can be simplified to

$$\mu_L^0 + RT \ln \theta_L = \frac{1}{2}\mu_{H_2}^0 + \frac{1}{2}RT \ln f_{H_2} \qquad (9)$$

The hydrogen concentration in lattice sites is obtained by substituting $\theta_L = C_L/N_L$ in Eq. (9)

$$C_L = S_L\sqrt{f_{H_2}} \qquad (10)$$

where $S_L = N_L \exp\left(\frac{\frac{1}{2}\mu_{H_2}^0 - \mu_L^0}{RT}\right)$. This expression represents the Sieverts' law.

In addition, the chemical potential of atomic hydrogen in trap sites (besides the voids) can be expressed as follows

$$\mu_T = \mu_T^0 + RT \ln \frac{\theta_T}{1 - \theta_T} \qquad (11)$$

where μ_T^0 is the chemical potential of trapped hydrogen in a reference state and θ_T is the occupancy of trap sites $\theta_T = C_T/N_T$ with C_T is the volume concentration of hydrogen in trap sites (m^{-3}) and N_T is the number of trap sites per unit volume (m^{-3}). In the same way, at equilibrium, the chemical potential of hydrogen inside the voids must be equal to the chemical potential of hydrogen in traps ($\frac{1}{2}\mu_{H_2} = \mu_T$) and assuming that $\theta_T \ll 1$, we obtain a similar equation to Eq. (10)

$$C_T = S_T\sqrt{f_{H_2}} \qquad (12)$$

where $S_T = N_T \exp\left(\frac{\frac{1}{2}\mu_{H_2}^0 - \mu_T^0}{RT}\right)$. It has to be mentioned that this equation is only valid in cases where the occupancy of trap sites is low.

Finally, considering that the "dissolved" hydrogen is a combination of lattice and trapped hydrogen ($C_{LT} = C_L + C_T$), it is possible to express the concentration of the "dissolved" hydrogen by combining Eq.10 and Eq.12

$$C_{LT} = S_{LT}\sqrt{f_{H_2}} \qquad (13)$$

33

where $S_{LT} = S_L + S_T$. Again an equation similar to Sieverts' law is obtained, provided that the trap occupancy is low.

VI Acknowledgements

VII Funding

VIII Data availability statement

The raw and processed data required to reproduce these findings are available from the corresponding author upon request.

IX References

[1] R. P. Frohmberg, W. J. Barnett, and A. R. Troiano, 'DELAYED FAILURE AND HYDROGEN EMBRITTLEMENT IN STEEL':, Defense Technical Information Center, Fort Belvoir, VA, Jun. 1954.

[2] J.-C. BOSSON, 'Analyse de l'hydrogène dans les aciers', 'Étude et propriétés des métaux', techniques de l'ingénieur Apr. 10, 1993..

[3] J. Fan, L. Yan, H. Zhou, and E. Cao, 'Variation of cavity hydrogen pressure in the forming process of heavy forging', Int. J. Adv. Manuf. Technol., vol. 89, no. 5, pp. 1259–1267, Mar. 2017.

[4] S. P. Lynch, 'Hydrogen embrittlement (HE) phenomena and mechanisms', in Stress Corrosion Cracking, Elsevier, 2011, pp. 90–130.

[5] S. K. Dwivedi and M. Vishwakarma, 'Hydrogen embrittlement in different materials: A review', Int. J. Hydrog. Energy, vol. 43, no. 46, pp. 21603–21616, Nov. 2018.

[6] Zapffe CA and Sims CE, 'Hydrogen embrittlement, internal stress and defects in steel', Trans AIME 145, pp. 225–261, 1941.

[7] M. Riedler, S. Michelic, and C. Bernhard, 'Formation of shrinkage porosity during solidification of steel: Numerical simulation and experimental validation', IOP Conf. Ser. Mater. Sci. Eng., vol. 143, p. 012035, Jul. 2016.

[8] R. D. Pehlke, 'Formation of Porosity During Solidification of Cast Metals', in Foundry Processes: Their Chemistry and Physics, S. Katz and C. F. Landefeld, Eds. Boston, MA: Springer US, 1988, pp. 427–445.

[9] J.-G. Sezgin, C. Bosch, A. Montouchet, G. Perrin, and K. Wolski, 'Modelling of hydrogen induced pressurization of internal cavities', Int. J. Hydrog. Energy, vol. 42, no. 22, pp. 15403–15414, Jun. 2017.

[10] C. Ly, 'Caractérisation d'aciers à très haute limite d'élasticité vis-à-vis de la fragilisation par l'hydrogène',PhD Thesis Éc. Cent. Paris, p. 191, 2009.

[11] J.-G. Sezgin, C. Bosch, A. Montouchet, G. Perrin, and K. Wolski, 'Modelling and simulation of hydrogen redistribution in a heterogeneous alloy during the cooling down to 200 °C', Int. J. Hydrog. Energy, vol. 42, no. 30, pp. 19346–19358, Jul. 2017.

[12] A.-M. BRASS, J. CHÊNE, and L. COUDREUSE, 'Fragilisation des aciers par l'hydrogène : étude et prévention', - 'Corrosion Vieillissement', techniques de l'ingénieur, Jun. 10, 2000.

[13] J. Rogers, 'Hydrogen-assisted cracking in carbon and low-alloy steel castings: Fracture, Analysis and Manufacture', Wis. Centrif. Div. Met. Int.

[14] M. Möser and V. Schmidt, 'FRACTOGRAPHY AND MECHANISM OF HYDROGEN CRACKING - THE FISHEYE CONCEPT', in Fracture 84, Elsevier, pp. 2459–2466, 1984

[15] A. R. Troiano, 'The Role of Hydrogen and Other Interstitials in the Mechanical Behavior of Metals', Metallogr. Microstruct. Anal., vol. 5, no. 6, pp. 557–569, Dec. 2016.

[16] T. Depover and K. Verbeken, 'Hydrogen trapping and hydrogen induced mechanical degradation in lab cast Fe-C-Cr alloys', Mater. Sci. Eng. A, vol. 669, pp. 134–149, Jul. 2016.

[17] D. Pérez Escobar, K. Verbeken, L. Duprez, and M. Verhaege, 'Evaluation of hydrogen trapping in high strength steels by thermal desorption spectroscopy', Mater. Sci. Eng. A, vol. 551, pp. 50–58, Aug. 2012.

[18] S. Frappart et al., 'Hydrogen trapping in martensitic steel investigated using electrochemical permeation and thermal desorption spectroscopy', Scr. Mater., vol. 65, no. 10, pp. 859–862, Nov. 2011.

[19] B. A. Szost, R. H. Vegter, and P. E. J. Rivera-Díaz-del-Castillo, 'Hydrogen-Trapping Mechanisms in Nanostructured Steels', Metall. Mater. Trans. A, vol. 44, no. 10, pp. 4542–4550, Oct. 2013

[20] A. H. M. Krom and A. Bakker, 'Hydrogen trapping models in steel', Metall. Mater. Trans. B, vol. 31, no. 6, pp. 1475–1482, Dec. 2000.

[21] J.-Y. Lee and J.-L. Lee, 'A trapping theory of hydrogen in pure iron', Philos. Mag. A, vol. 56, no. 3, pp. 293–309, Sep. 1987.

[22] S.-M. Lee and J.-Y. Lee, 'Hydrogen trapping by voids in nickel', Scr. Metall., vol. 21, no. 12, pp. 1655–1658, Dec. 1987.

[23] G. Padhy, 'Diffusible hydrogen in steel weldments - a status review', Accessed: Jun. 09, 2021. [Online]. Available: https://www.academia.edu/8767562/Diffusible_hydrogen_in_steel_weldments_a_status_review

[24] W. Y. Choo and J. Y. Lee, 'Thermal analysis of trapped hydrogen in pure iron', Metall. Trans. A, vol. 13, no. 1, pp. 135–140, Jan. 1982.

[25] A. Oudriss, F. Martin, and X. Feaugas, '11 - Experimental Techniques for Dosage and Detection of Hydrogen', in Mechanics - Microstructure - Corrosion Coupling, C. Blanc and I. Aubert, Eds. Elsevier, pp. 245–268, 2019.

[26] K. Verbeken, '2 - Analysing hydrogen in metals: bulk thermal desorption spectroscopy (TDS) methods', in Gaseous Hydrogen Embrittlement of Materials in Energy Technologies, vol. 1, R. P. Gangloff and B. P. Somerday, Eds. Woodhead Publishing, pp. 27–55, 2012.

[27] R. Rizzo, S. Baier, M. Rogowska, and R. Ambat, 'An electrochemical and X-ray computed tomography investigation of the effect of temperature on CO2 corrosion of 1Cr carbon steel', Corros. Sci., vol. 166, p. 108471, Apr. 2020.

[28] B. Wolf, 'Application of hydrostatic weighing to density determination of tiny porous samples', Rev. Sci. Instrum., vol. 66, no. 3, p. 2578, Jun. 1998.

[29] M. A. V. Devanathan and Z. Stachurski, 'The Adsorption and Diffusion of Electrolytic Hydrogen in Palladium', Proc. R. Soc. Lond. Ser. Math. Phys. Sci., vol. 270, no. 1340, pp. 90–102, 1962.

[30] M. J. Danielson, 'Use of the Devanathan–Stachurski cell to measure hydrogen permeation in aluminum alloys', Corros. Sci., vol. 44, no. 4, pp. 829–840, Apr. 2002.

[31] A. Oudriss, F. Martin, and X. Feaugas, 'Experimental Techniques for Dosage and Detection of Hydrogen', in Mechanics - Microstructure - Corrosion Coupling, Elsevier, pp. 245–268, 2019.

[32] M. Ichiba, J. Sakai, T. Doshida, and K. Takai, 'Corrosion reaction and hydrogen absorption of steel for prestressed concrete in a 20mass% ammonium thiocyanate solution', Scr. Mater., vol. 102, pp. 59–62, Jun. 2015

[33] M. Nagumo, K. Takai, and N. Okuda, 'Nature of hydrogen trapping sites in steels induced by plastic deformation', J. Alloys Compd., vol. 293–295, pp. 310–316, Dec. 1999.

[34] A. K. Belyaev, A. M. Polyanskiy, V. A. Polyanskiy, Ch. Sommitsch, and Yu. A. Yakovlev, 'Multichannel diffusion vs TDS model on example of energy spectra of bound hydrogen in 34CrNiMo6 steel after a typical heat treatment', Int. J. Hydrog. Energy, vol. 41, no. 20, pp. 8627–8634, Jun. 2016.

[35] E. Tal-Gutelmacher, D. Eliezer, and E. Abramov, 'Thermal desorption spectroscopy (TDS)—Application in quantitative study of hydrogen evolution and trapping in crystalline and non-crystalline materials', Mater. Sci. Eng. A, vol. 445–446, pp. 625–631, Feb. 2007.

[36] S. Yamasaki, T. Manabe, and D. Hirakami, 'Analysis of Hydrogen State in Steel and Trapping Using Thermal Desorption Method', Nippon steel and Sumitomo metal technical report no. 116, p. 6, 2017.

[37] C. V. Tapia-Bastidas, A. Atrens, and E. MacA. Gray, 'Thermal desorption spectrometer for measuring ppm concentrations of trapped hydrogen', Int. J. Hydrog. Energy, vol. 43, no. 15, pp. 7600–7617, Apr. 2018.

[38] J. Venezuela et al., 'Determination of the equivalent hydrogen fugacity during electrochemical charging of 3.5NiCrMoV steel', Corros. Sci., vol. 132, pp. 90–106, Mar. 2018.

[39] Z. Silvestri et al., 'Thermal desorption mass spectrometer for mass metrology', Rev. Sci. Instrum., vol. 85, no. 4, p. 045111, Apr. 2014.

[40] M. A. Liu, P. E. J. Rivera-Díaz-del-Castillo, J. I. Barraza-Fierro, H. Castaneda, and A. Srivastava, 'Microstructural influence on hydrogen permeation and trapping in steels', Mater. Des., vol. 167, p. 107605, Apr. 2019.

[41] A. Helmi, 'Sieverts' Law', in Encyclopedia of Membranes, E. Drioli and L. Giorno, Eds. Berlin, Heidelberg: Springer, pp. 1–2, 2015.

[42] S. L. I. Chan and J. A. Charles, 'Effect of carbon content on hydrogen occlusivity and embrittlement of ferrite–pearlite steels', Mater. Sci. Technol., vol. 2, no. 9, pp. 956–962, Sep. 1986.

[43] K. Takai and R. Watanuki, 'Hydrogen in Trapping States Innocuous to Environmental Degradation of High-strength Steels', ISIJ Int., vol. 43, no. 4, pp. 520–526, 2003.

[44] J. S. Kim, Y. H. Lee, D. L. Lee, K.-T. Park, and C. S. Lee, 'Microstructural influences on hydrogen delayed fracture of high strength steels', Mater. Sci. Eng. A, vol. 505, no. 1, pp. 105–110, Apr. 2009.

[45] H. Husby, M. Iannuzzi, R. Johnsen, M. Kappes, and A. Barnoush, 'Effect of nickel on hydrogen permeation in ferritic/pearlitic low alloy steels', Int. J. Hydrog. Energy, vol. 43, no. 7, pp. 3845–3861, Feb. 2018.

[46] S. Takagi, Y. Toji, M. Yoshino, and K. Hasegawa, 'Hydrogen Embrittlement Resistance Evaluation of Ultra High Strength Steel Sheets for Automobiles', ISIJ Int., vol. 52, no. 2, pp. 316–322, 2012.

[47] R. W. Pasco and P. J. Ficalora, 'The adsorption of hydrogen on iron; A surface orbital modified occupancy — bond energy bond order calculation', Surf. Sci., vol. 134, no. 2, pp. 476–498, Nov. 1983.

[48] K. C. Wong, 'Void trapping of hydrogen in sintered iron', Master Thesis, Jan. 09, 1976. https://digital.library.unt.edu/ark:/67531/metadc1444559/ (accessed Jun. 06, 2021).

[49] C. S. Marchi, B. P. Somerday, and S. L. Robinson, 'Permeability, solubility and diffusivity of hydrogen isotopes in stainless steels at high gas pressures', Int. J. Hydrog. Energy, vol. 32, no. 1, pp. 100–116, Jan. 2007.

[50] A. Sieverts, 'Absorption of Gases by Metals', Zeitschrift für Metallkunde, Vol. 21, pp. 37-46 1929.